Received: 8 October 2019 | Revised: 2 November 2019 | Accepted: 24 November 2019

DOI: 10.1111/jace.16939

ORIGINAL ARTICLE

Journal of the American Ceramic Society

Multifunctional optical thermometry based on the stark sublevels of Er^{3+} in CaO-Y_2O_3: Yb^{3+}/Er^{3+}

Guotao Xiang[1] | **Xiaotong Liu**[1] | **Wen Liu**[4] | **Bin Wang**[3] | **Zhen Liu**[1] | **Sha Jiang**[1] | **Xianju Zhou**[1] | **Li Li**[1] | **Ye Jin**[5] | **Jiahua Zhang**[2]

[1]Department of Mathematics and Physics, Chongqing University of Posts and Telecommunications, Chongqing, China

[2]State Key Laboratory of Luminescence and Applications, Changchun Institute of Optics, Fine Mechanics and Physics, Chinese Academy of Sciences, Changchun, China

[3]Information and Network Management Center, Chongqing University of Posts and Telecommunications, Chongqing, China

[4]College of Physics, Liaoning University, Shenyang, China

[5]School of Science, Chongqing University of Technology, Chongqing, China

Correspondence
Guotao Xiang, Department of Mathematics and Physics, Chongqing University of Posts and Telecommunications, 2 Chongwen Road, Chongqing 400065, China.
Email: xianggt@cqupt.edu.cn

Jiahua Zhang, State Key Laboratory of Luminescence and Applications, Changchun Institute of Optics, Fine Mechanics and Physics, Chinese Academy of Sciences, 3888 Eastern South Lake Road, Changchun 130033, China
Email: zhangjh@ciomp.ac.cn

Funding information
National Natural Science Foundation of China, Grant/Award Number: 11604037, 11674044 and 11704054; Science and Technology Research Program of Chongqing Municipal Education Commission, Grant/Award Number: KJZD-K201800602; Chongqing Research Program of Basic Research and Frontier Technology, Grant/Award Number: CSTC2016jcyjA0113 and CSTC2017jcyjAX0046

Abstract

A conventional high temperature solid state method was utilized to prepare CaO-Y_2O_3, which is a potential candidate for manufacturing crucible material to melt titanium and titanium alloys with low cost. Meanwhile, Yb^{3+} ions and Er^{3+} ions were selected as the sensitizers and activators respectively to dope into CaO-Y_2O_3, aimed at providing real-time optical thermometry during the preparation process of titanium alloys realized using fluorescence intensity ratio (FIR) technology. The results reveal that a high measurement precision can be acquired by using the Stark sublevels of Er^{3+} $^4F_{9/2}$ to measure the temperature with a maximum absolute error of only about 3 K. In addition, by analyzing the dependence of $^4I_{13/2} \rightarrow {}^4I_{15/2}$ transition on pump power of 980 nm excitation wavelength, it was found that the laser-induced thermal effect has almost no influence on the temperature measurement conducted by using the FIR of the Stark sublevels of Er^{3+} $^4I_{13/2}$, which means that a high excitation pump power can be used to obtain strong NIR emission and good signal-to-noise ratio for optical thermometry without the influence of the laser-induced thermal effect. All the results reveal that CaO-Y_2O_3: Yb^{3+}/Er^{3+} is an excellent temperature sensing material with high measurement precision.

KEYWORDS

fluorescence intensity ratio, optical thermometry, upconversion, Yb^{3+}/Er^{3+}

1 | INTRODUCTION

Nowadays, titanium is one kind of a very important structural metal. Titanium alloys possess high specific strength, excellent heat stability and strong corrosion resistance, and are widely applied in every field, such as the aerospace industry, automobile industry, biomedicine and so on.[1,2] Nevertheless, titanium and titanium alloys can react with almost all kinds of refractory compounds (such as Al_2O_3, MgO, etc) to produce brittle materials due to their high chemical activity under molten state, which results in a complex melting process and high cost to generate titanium alloys.[3,4] To date, it is also a great challenge to choose a suitable crucible material for melting titanium and titanium alloys.

CaO may be a potential candidate for manufacturing crucible material to melt titanium and titanium alloys thanks to its high melting point and excellent thermodynamic properties. For instance, Sun et al have reported that TiNi alloy can been fabricated very well in CaO crucibles without pollution.[5] Recently, the poor hydration resistance of CaO crucible in the air, which is a serious limitation for its industrial application, has also been improved enormously by Meng's group realized with rare-earth sesquioxide Y_2O_3 doping.[6] More importantly, there is no reaction between CaO-Y_2O_3 and titanium alloys.

Besides crucible material, temperature is a very important physical parameter during the preparation process of titanium alloys. In the metallurgical industry, it is necessary to measure temperature with rapid speed and high precision. Optical thermometry may be a perfect choice to satisfy these requirements. Compared with conventional methods of temperature measurements, optical thermometry can realize a spatial distribution of temperature with sub-micrometer resolution. Meanwhile, optical thermometry also owns merits such as rapid response, non-contact, strong anti-jamming capability and so on.[7–15] At present, the research hotspot about optical thermometry mainly focuses on fluorescence intensity ratio (FIR) technology utilizing pairs of thermally coupled energy levels in rare-earth ions.[16–19] More specifically, the two thermally coupled energy levels used in FIR technology are closely separated, so the upper level can be populated from the lower level by a thermal excitation process at higher temperature.[20] In this case, the FIR of the two thermally coupled levels can be fitted well by Boltzmann equation and then the temperature measurement can be realized. There are a series of thermally coupled energy levels existing in rare-earth ions, such as Er^{3+}: $^2H_{11/2}/^4S_{3/2}$ levels, Tm^{3+}: $^3F_{2,3}/^3H_4$ levels, Eu^{3+}: $^5D_0/^5D_1$ levels, etc[21–27]

In this paper, CaO-Y_2O_3: Yb^{3+}/Er^{3+} were synthesized using a conventional high temperature solid state method. Yb^{3+} ions and Er^{3+} ions were selected as the sensitizers and activators respectively to use for temperature measurement, aimed at providing a real-time optical thermometry during the preparation process of titanium alloys. The optimal doping concentration of Yb^{3+} ions and Er^{3+} ions in CaO-Y_2O_3 have been explored. Meanwhile, the thermometry behaviors based on the Stark sublevels of Er^{3+} $^4F_{9/2}$ and $^4I_{13/2}$ have been studied in detail. In addition, since the raw materials Yb_2O_3 and Er_2O_3 possess similar physicochemical properties to Y_2O_3, the doped Yb^{3+} ions and Er^{3+} ions in CaO-Y_2O_3 should have no effect on the application of manufacturing crucible material to melt titanium and titanium alloys. All the results reveal that CaO-Y_2O_3: Yb^{3+}/Er^{3+} is a promising candidate that can realize an accurate optical thermometry.

2 | EXPERIMENTAL

2.1 | Chemicals

Y_2O_3 (99.99%), Yb_2O_3 (99.99%), and Er_2O_3 (99.99%) were purchased from Yangkou state-run rare-earth company. Analytical grade $CaCO_3$ was obtained from Chongqing Chuandong Chemical (Group) Co, Ltd. All of the oxides were used as raw materials without further treatment.

2.2 | Preparation

The CaO-Y_2O_3: y % Yb^{3+}/x % Er^{3+} were synthesized using a conventional high temperature solid state method, specific as follows. Firstly, the raw materials were weighed in stoichiometric proportion. Secondly, they were mixed homogeneously for 30 minutes in an agate mortar and then the mixtures were put in a crucible. Finally, the powders were preheated in a furnace at 800°C for 3 hours, followed by further sintering at 1600°C for 5 hours to get the final samples. Here, it is necessary to note that the total concentration of Re^{3+} ions (Re^{3+} = Y^{3+}, Yb^{3+}, Er^{3+}) is 10%, which is relative to Ca^{2+} ions. Relative to Y^{3+} ions, the concentration of Yb^{3+} ions and Er^{3+} ions is y % and x % (x = 0, 1, 2, 3, 4, 5, 6; y = 0, 1, 5, 10, 20, 30), respectively.

2.3 | Characterization

A Persee XD-2 diffractometer supplied by Beijing Purkinje General Instrument Co., Ltd was used to record the powder X-ray diffraction (XRD) data. The spectral data were collected using a FLS920 spectrometer purchased from Edinburgh Instruments.

3 | RESULTS AND DISCUSSION

3.1 | Structure

The XRD patterns of CaO-Y_2O_3 and CaO-Y_2O_3: 10% Yb^{3+}/4% Er^{3+} are presented in Figure 1. Congruously,

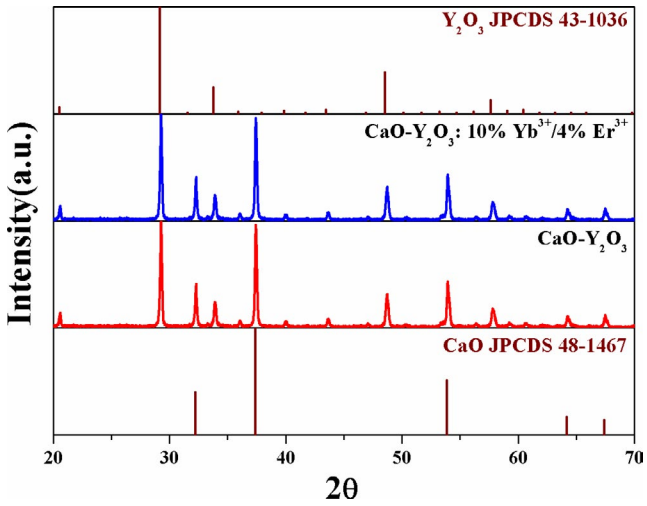

FIGURE 1 The X-ray diffraction (XRD) patterns of CaO-Y_2O_3 and CaO-Y_2O_3: 10% Yb^{3+}/4% Er^{3+} with the standard XRD data of CaO (JCPDS 48-1467) and Y_2O_3 (JCPDS 43-1036)

the intensities and positions of the diffraction peaks for each sample match well with the standard cards of CaO (JCPDS 48-1467) and Y_2O_3 (JCPDS 43-1036), demonstrating the successful preparation of the target product without other impure phases. Moreover, the two samples show similar XRD patterns, indicating that Yb^{3+} and Er^{3+} are all incorporated into Y_2O_3 and formed a solid solution structure.

3.2 | Luminescence properties

3.2.1 | The UC properties of CaO-Y_2O_3: Yb^{3+}/Er^{3+}

In order to explore the optimal doping concentration of Yb^{3+} and Er^{3+} in CaO-Y_2O_3, samples doped with various Yb^{3+} and Er^{3+} concentrations were prepared and the corresponding UC spectra were also measured and are displayed in Figure 2A,B. Obviously, excited by 980 nm wavelength, two weak green emission bands and a strong red emission band exhibit in the range of 500-700 nm, which originate from $^2H_{11/2} \rightarrow {}^4I_{15/2}$ transition located at 522 nm, $^4S_{3/2} \rightarrow {}^4I_{15/2}$ transition located at 564 nm and $^4F_{9/2} \rightarrow {}^4I_{15/2}$ transition located at 661 nm of Er^{3+}, respectively. Meanwhile, by fixing the doping concentration of Yb^{3+} and Er^{3+} respectively, the optimal doping concentrations of Yb^{3+} and Er^{3+} for the strongest UC emission were determined to be 10% and 4%. In addition, although the variable doping concentration of Yb^{3+} and Er^{3+} had no effect on the position of the three emission bands, the UC intensity dramatically changed. As depicted in Figure 2B, the red UC intensity is enhanced by a factor of 19, resulting from the efficient energy transfer (ET) from sensitizer Yb^{3+} to activator Er^{3+}. Figure 2C shows the near-infrared (NIR) emission spectra of CaO-Y_2O_3: 20% Yb^{3+}/x % Er^{3+} excited by 980 nm wavelength. In this region, the spectra are composed of two bands, corresponding to the $^2F_{5/2} \rightarrow {}^2F_{7/2}$ transition located at 1028 nm of Yb^{3+} and $^4I_{13/2} \rightarrow {}^4I_{15/2}$ transition located at 1534 nm of Er^{3+}. Clearly, the emission intensity of $^2F_{5/2} \rightarrow {}^2F_{7/2}$ transition of Yb^{3+} is reduced distinctly with the increase of Er^{3+} doping concentration, which is a direct proof for the efficient ET between the Yb^{3+} ions and Er^{3+} ions.

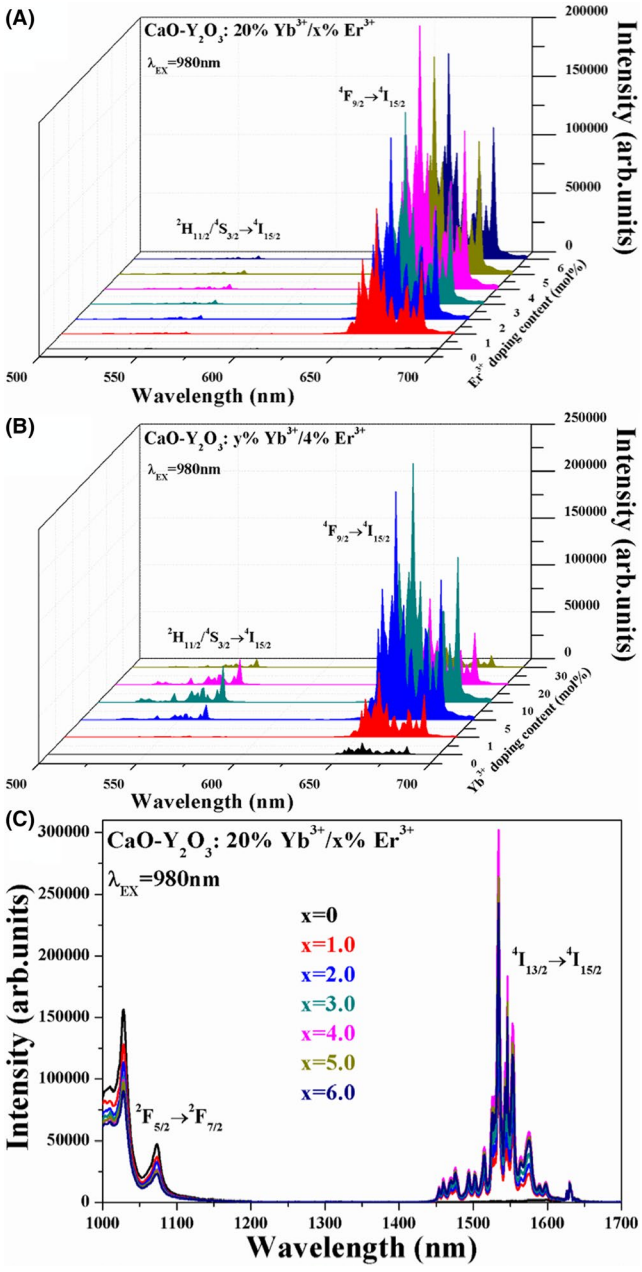

FIGURE 2 The UC spectra of (A) CaO-Y_2O_3: 20% Yb^{3+}/x % Er^{3+} (x = 0, 1, 2, 3, 4, 5, 6) and (B) CaO-Y_2O_3: y % Yb^{3+}/4% Er^{3+} (y = 0, 1, 5, 10, 20, 30). (C) The NIR spectra of CaO-Y_2O_3: 20% Yb^{3+}/x % Er^{3+}

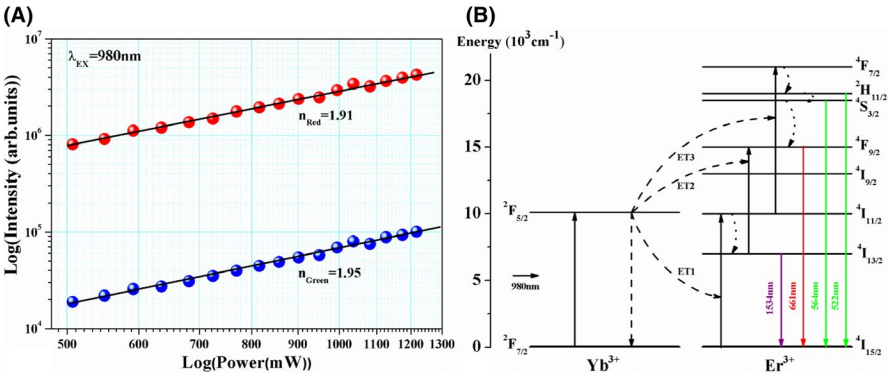

FIGURE 3 A, Double logarithmic relationship of green and red UC emission versus excitation power in CaO-Y_2O_3: 10% Yb^{3+}/4% Er^{3+}. B, The energy level diagram with the related ET processes

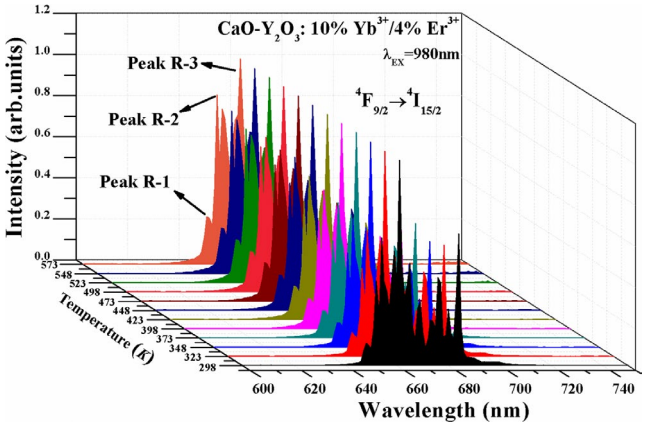

FIGURE 4 Temperature dependence of UC spectra in CaO-Y_2O_3: 10% Yb^{3+}/4% Er^{3+} excited by 980 nm wavelength with low excitation power. The UC intensities of Peak R-3 are normalized

To further investigate the UC mechanism in CaO-Y_2O_3: Yb^{3+}/Er^{3+}, the dependence of the UC intensity on pump power was measured and is displayed in Figure 3A. The calculated slopes for green and red UC emissions are 1.91 and 1.95 respectively, revealing that both green and red UC emission are a two-photon process. Based on the above phenomenon, the energy level diagram of Yb^{3+} ions and Er^{3+} ions with the possible ET processes is schematically described in Figure 3B.[28,29] Excited by 980 nm wavelength, Yb^{3+} ions at the ground state can be excited to $^2F_{5/2}$ level by a ground state absorption process. Then Er^{3+} ions in the ground state can be populated to $^4I_{11/2}$ level by receiving energy from the excited Yb^{3+} ions (ET1). Subsequently, the green emitting states $^2H_{11/2}$/$^4S_{3/2}$ of Er^{3+} ions can be populated by obtaining energy again from the excited Yb^{3+} ions (ET3) along with a multi-phonon relaxation (MPR) process. The Er^{3+} ions at $^4I_{11/2}$ level can also be de-excited to $^4I_{13/2}$ level by a MPR process. Then the red emitting state $^4F_{9/2}$ of Er^{3+} ions can be populated through ET2 process. In addition, the MPR process from $^4S_{3/2}$ of Er^{3+} ions is also a route for populating $^4F_{9/2}$ level.

3.2.2 | The optical thermometry behaviors of CaO-Y_2O_3: Yb^{3+}/Er^{3+}

In most previous papers about UC optical thermometry, the thermally coupled levels $^2H_{11/2}$ and $^4S_{3/2}$ of Er^{3+} ions were the most commonly used due to the excellent UC properties and suitable energy gap. However, definitely, in this work, this pair of thermally coupled levels is hard to apply to temperature sensing because of the weak green UC emission. Actually, the thermally coupled red Stark sublevels of Er^{3+} $^4F_{9/2}$ manifold can also be employed to measure the temperature with perfect sensitivity.[30,31]

Subsequently, in order to investigate the temperature sensing behavior based on the thermally coupled red Stark sublevels, the thermal evolution red UC emission spectra of CaO-Y_2O_3: 10% Yb^{3+}/4% Er^{3+} were measured and are shown in Figure 4. There are several emission peaks existing in the range of 600-700 nm, which belong to the Stark transitions of $^4F_{9/2} \rightarrow {}^4I_{15/2}$ transition. It is necessary to note that the emission intensities at 661 nm (named Peak R-3) have been normalized to 1. Intuitively, the intensities of almost all the peaks are increased relative to Peak R-3 with increasing temperature. That is to say, the variation rate of Peak R-3 is smaller than that of the other peaks, which makes it possible to measure the temperature by utilizing FIR between these red Stark sublevels. Here, Peak R-1 (located at 648 nm), Peak R-2 (located at 652 nm) and Peak R-3 were chosen as the targets for optical thermometry. The Boltzmann-type distribution law can be expressed as:

$$\mathrm{FIR} = I_2/I_1 = B\exp(-\Delta E/k_B T), \quad (1)$$

with $B = g_1\upsilon_1\sigma_1/g_2\upsilon_2\sigma_2$. Here, I_1 and I_2 are the integrated intensities of the lower level and the upper level, respectively. k_B and T define the Boltzmann constant and absolute temperature. The degeneracy degree, spontaneous emission, and absorption rate are symbolized as g, υ and σ respectively. Based on Equation (1), the variation of FIR_1 between Peak R-1 and Peak R-3 with absolute temperature can be expressed as follows (see Figure 5A):

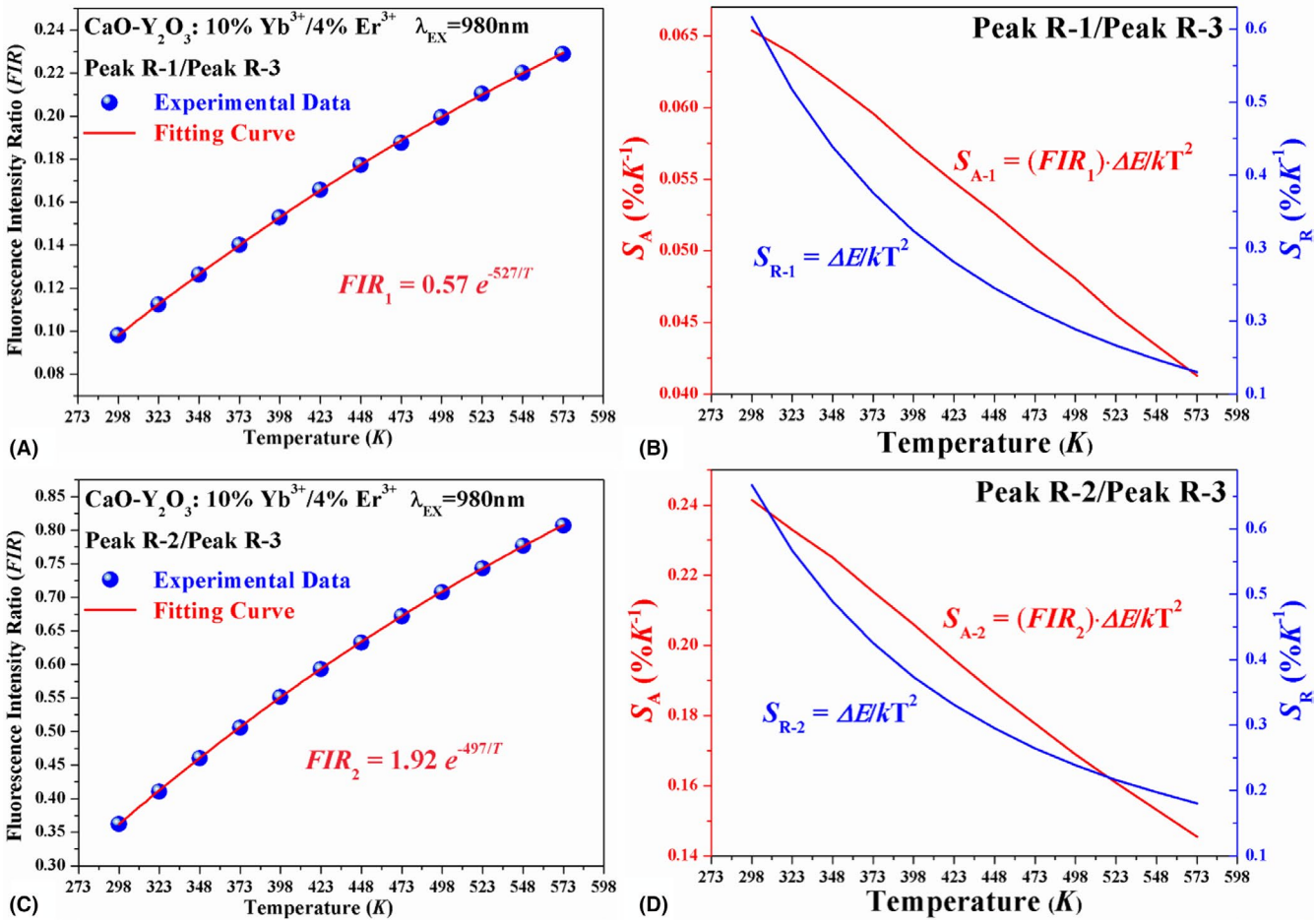

FIGURE 5 Temperature dependence of (A) FIR_1 between Peak R-1 and Peak R-3, (B) $S_{A\text{-}1}$ and $S_{R\text{-}1}$, (C) FIR_2 between Peak R-2 and Peak R-3 and (D) $S_{A\text{-}2}$ and $S_{R\text{-}2}$ in CaO-Y_2O_3: 10% Yb^{3+}/4% Er^{3+}

$$\mathrm{FIR}_1 = 0.57 \exp(-527/T), \tag{2}$$

Since $\Delta E/k_B = 527$, the calculated ΔE between Peak R-1 and Peak R-3 is approximately 366 cm^{-1}. Compared with the ΔE value obtained from the UC emission spectra (304 cm^{-1}), the error of ΔE is 62 cm^{-1}, resulting from the enhancement of the MPR and ET at high temperature.[32] The absolute sensitivity S_A and relative sensitivity S_R, which are the vital parameters to evaluate the optical thermometry materials, can be calculated by the following expression:

$$S_A = |d(\mathrm{FIR})/dT| = (\mathrm{FIR}) \cdot (\mathrm{DE}/k_B T^2), \tag{3}$$

$$S_R = |d(\mathrm{FIR})/(\mathrm{FIR}) \cdot dT| = \mathrm{DE}/k_B T^2. \tag{4}$$

The corresponding values of sensor sensitivity as a function of temperature were calculated and are depicted in Figure 5B. The values of both S_A and S_R keep decreasing in the testing range from 298 to 573 K, which achieve the maximum 0.65 × 10^{-3} K^{-1} and 6.67 × 10^{-3} K^{-1} respectively at the beginning temperature. In addition, the FIR_2 between Peak R-2 and Peak R-3 can also be used to measure the temperature, which owns similar properties to FIR_1, as shown in Figure 5C,D. The repeatability study in the temperature cycling between 298 and 573 K for the

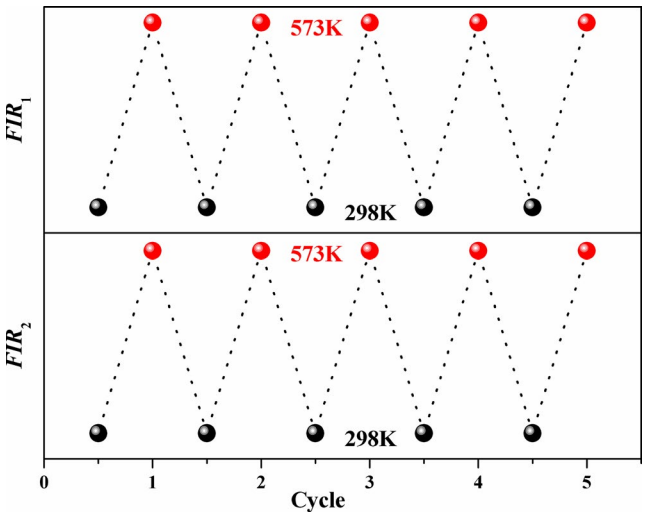

FIGURE 6 The repeatability study in the temperature cycling between 298 and 573 K

Stark transitions of $^4F_{9/2} \rightarrow {}^4I_{15/2}$ transition is shown in Figure 6. The FIR_1 of Peak R-1 and Peak R-3 and FIR_2 of Peak R-2 and Peak R-3 were almost unchanged in the cycling process. It indicates the excellent repeatability and reliability of this material.

In order to evaluate the accuracy of optical thermometry in this work, two approaches were used to determine the temperature. To be specific, as shown in Figure 7A, a heating gun was used to heat the sample CaO-Y_2O_3: 10% Yb^{3+}/4% Er^{3+} to a certain temperature and then the UC spectrum was collected using a spectrometer at 980 nm wavelength excitation. At the same time, an infrared thermometer was also utilized as a contrast to record the temperature. The temperature calculated by FIR_1 and FIR_2 as well as the data recorded by the infrared thermometer are all plotted in Figure 7B. Fortunately, the values of temperature whether deduced by FIR_1 or FIR_2 match well with the data recorded by the infrared thermometer, demonstrating the high accuracy of CaO-Y_2O_3: 10% Yb^{3+}/4% Er^{3+} for optical thermometry. The maximum absolute error for FIR_1 and FIR_2 is 3.1 and 3.2 K, respectively.

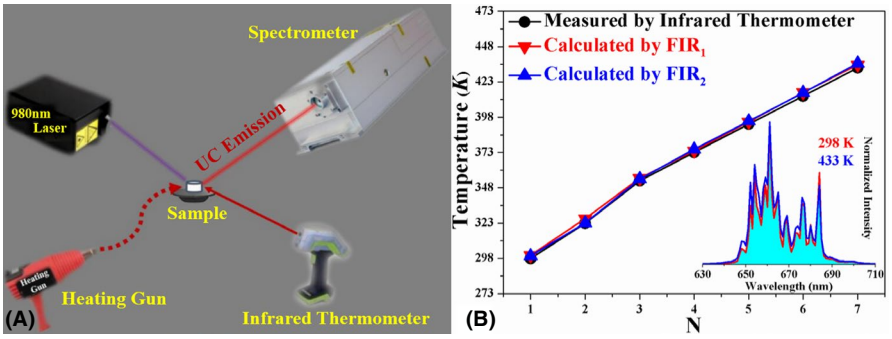

FIGURE 7 A, Scheme of the setup for the temperature determination experiment. B, The temperature calculated by FIR_1 and FIR_2 as well as detected using an infrared thermometer. Inset, the red UC spectra with normalized intensity measured at 298 and 433 K

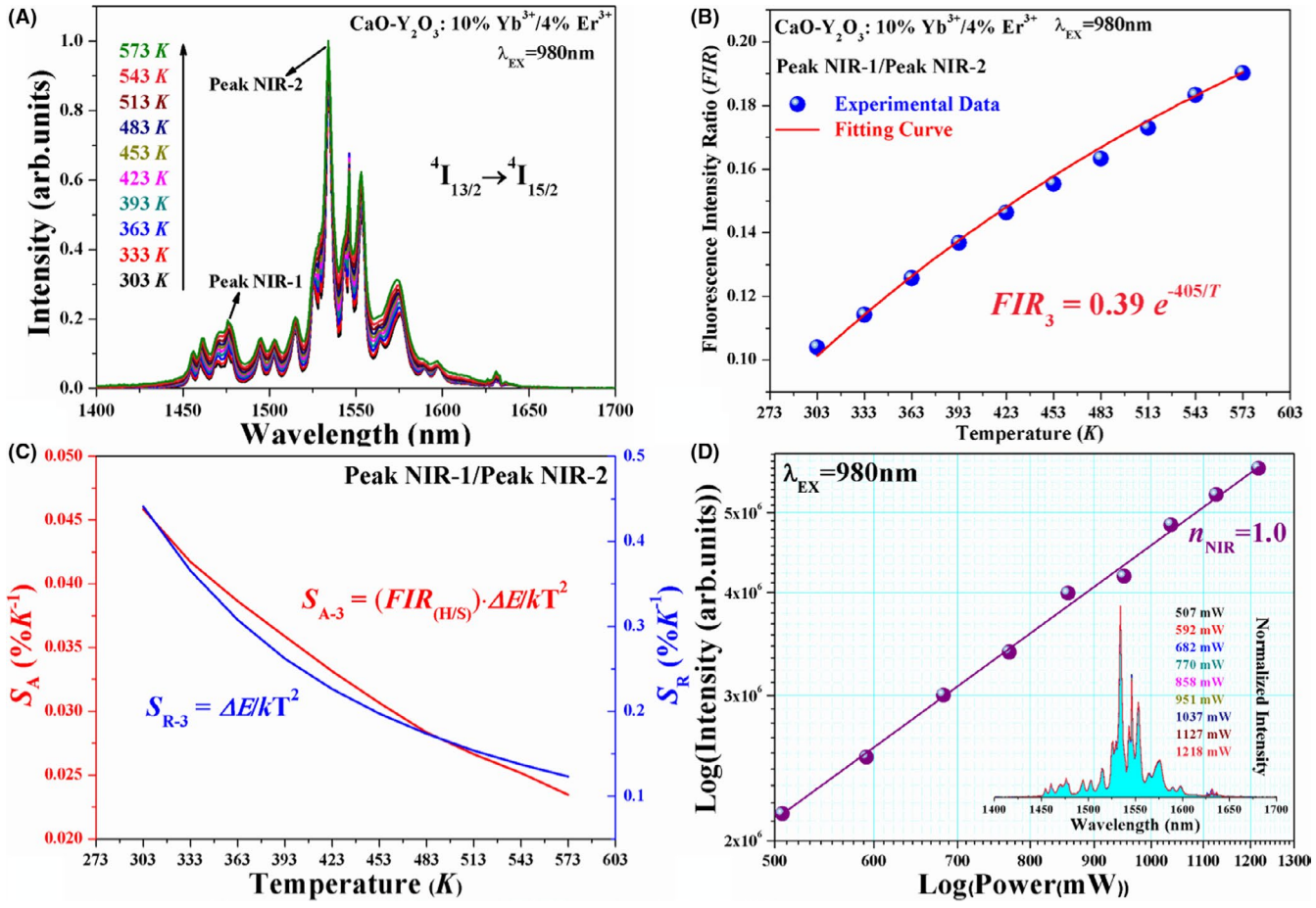

FIGURE 8 Temperature dependence of (A) $^4I_{13/2} \rightarrow {}^4I_{15/2}$ transition, (B) FIR_3 between Peak NIR-1 and Peak NIR-2 and (C) the corresponding $S_{A\text{-}3}$ and $S_{R\text{-}3}$. (D) Double logarithmic relationship of $^4I_{13/2} \rightarrow {}^4I_{15/2}$ transition versus excitation power. Inset, the corresponding NIR spectra with normalized intensity excited by various pump power

Beyond that, the relationship of $^4I_{13/2} \rightarrow {}^4I_{15/2}$ transition versus temperature in CaO-Y_2O_3: 10% Yb^{3+}/4% Er^{3+} has also been explored. As illustrated in Figure 8A, several emission peaks exist in the range of 1400-1700 nm, originating from the Stark transitions of $^4I_{13/2} \rightarrow {}^4I_{15/2}$ transition. The intensities of Peak NIR-2 (at 1534 nm) have been normalized to 1. The relative intensities of the other peaks change regularly with the rising temperature. Here, Peak NIR-1 (at 1476 nm) and Peak NIR-2, which derive from a pair of the thermally coupled Stark sublevels with a small energy separation between them ($\Delta E = 256$ cm^{-1}, calculated from the emission spectra), were chosen as targets for optical thermometry. Based on the Boltzmann-type distribution law, the variation of FIR_3 between Peak NIR-1 and Peak NIR-2 with absolute temperature can be written as follows (see Figure 8B).

$$FIR_3 = 0.39 \exp(-405/T), \quad (5)$$

According to the above fitting equation, the calculated ΔE between Peak NIR-1 and Peak NIR-2 is approximately 281 cm^{-1}, which is similar to the value obtained from the NIR emission spectra. The corresponding $S_{A\text{-}3}$ and $S_{R\text{-}3}$ are also calculated and are depicted in Figure 8C. The values of $S_{A\text{-}3}$ and $S_{R\text{-}3}$ keep decreasing in the testing range with the maximum 0.46×10^{-3} K^{-1} and 4.41×10^{-3} K^{-1} respectively at the beginning temperature.

Generally, in order to ensure the high sensitivity of UC optical thermometry, the excitation power should be low enough to avoid the laser-induced thermal effect.[32–34] Actually, the negative impact of this thermal effect mainly occurs in the multi-photon UC process with little influence on a one-photon luminescence process.[35] Figure 8D shows the dependence of $^4I_{13/2} \rightarrow {}^4I_{15/2}$ transition on pump power of 980 nm excitation wavelength, indicating a one-photon process for $^4I_{13/2} \rightarrow {}^4I_{15/2}$ transition. Meanwhile, as observed from the illustration in Figure 8D, the relative intensity of every Stark transition almost has no change with increasing pump power, which means that a high excitation pump power can be used to obtain strong NIR emission and a good signal-to-noise ratio for optical thermometry without the influence of the laser-induced thermal effect.

Indeed, the purpose of this work was to provide a real-time optical thermometry during the preparation process of titanium alloys realized using FIR technology. However, restricted by the condition of characterization, the highest testing temperature for optical thermometry in this work is only about 600 K, which is far below the melting temperature ~1800 K of titanium alloys. At present, the highest testing temperature for optical thermometry reported in the previous literature is approximately 1000 K, which is also restricted by the condition of characterization.[36] Nevertheless, we believe that CaO-Y_2O_3: Yb^{3+}/Er^{3+} would own excellent temperature sensing performance at high temperatures because of its good thermodynamic property and strong UC emission.

4 | CONCLUSIONS

In summary, the optical thermometry behaviors of CaO-Y_2O_3: Yb^{3+}/Er^{3+} based on the Stark sublevels of Er^{3+} $^4F_{9/2}$ and $^4I_{13/2}$ have been investigated in detail. The results reveal that a high measurement precision can be obtained by utilizing the Stark sublevels of Er^{3+} $^4F_{9/2}$ to measure the temperature with a maximum absolute error of only about 3 K. Besides that, we found that the laser-induced thermal effect has almost no influence on the temperature measurement conducted by using the FIR of the Stark sublevels of Er^{3+} $^4I_{13/2}$, which means that a high excitation pump power can be used to obtain strong NIR emission and good signal-to-noise ratio for optical thermometry. Briefly, it can be proposed that CaO-Y_2O_3: Yb^{3+}/Er^{3+} is an excellent temperature sensing material with high measurement precision.

ACKNOWLEDGMENTS

This work was financially supported by the National Natural Science Foundation of China (11674044, 11604037, 11704054), the Chongqing Research Program of Basic Research and Frontier Technology (CSTC2016jcyjA0113, CSTC2017jcyjAX0046) and the Science and Technology Research Program of Chongqing Municipal Education Commission (KJZD-K201800602).

ORCID

Guotao Xiang https://orcid.org/0000-0003-3587-6654
Sha Jiang https://orcid.org/0000-0001-7336-2115
Xianju Zhou https://orcid.org/0000-0002-8050-9688
Li Li https://orcid.org/0000-0003-1163-5733
Ye Jin https://orcid.org/0000-0002-2147-127X

REFERENCES

1. Cai W, Meng XL, Zhao LC. Recent development of TiNi-based shape memory alloys. Curr Opin Solid State Mater Sci. 2005;9(6):296–302.
2. Osman M, Guo B, Tong YX, Chen F, Tian B, Li L, et al. Recent development of bulk ultrafine grained TiNi-based shape memory alloys processed by severe plastic deformation. Rare Metal Mat Eng. 2014;43(6):1511–7.
3. Melting A. Melting, casting and forging problems in titanium alloys. Mater Sci Eng A. 1998;243(1–2):257–62.
4. Sikka VK, Wilkening D, Liebetrau J, Mackeyc B. Melting and casting of FeAl-based cast alloy. Mater Sci Eng A. 1998;258(1–2):229–35.
5. Sun TT, Jiang M, Li CH, Lu XG, Liu WD. Modification of CaO refractory for melting titanium alloys and its hydration resistance. Adv Mater Res. 2011;177:502–5.
6. Meng FL, Cheng ZW, Chen GY, Lu XG, Li CH, et al. Hydration resistance of Y_2O_3 doped CaO and its application to melting titanium alloys. In: Ikhmayies SJ, Li BW, Carpenter JS, Hwang JY, Monteiro SN, Li J, editors. Characterization of minerals, metals, and materials. Cham: Springer, 2016; p. 745–52.
7. Cheng Y, Gao Y, Lin H, Huang F, Wang YS. Strategy design for ratiometric luminescence thermometry: circumventing

the limitation of thermally coupled levels. J Mater Chem C. 2018;6(28):7462–78.
8. Li DY, Tian LL, Huang Z, Shao LX, Quan J, Wang YX. Optical temperature sensor based on infrared excited green upconversion emission in hexagonal phase $NaLuF_4$:Yb^{3+}/Er^{3+} nanorods. J Nanosci Nanotechnol. 2016;16(4):3641–5.
9. Gao Y, Cheng Y, Hu T, Ji Z, Lin H, Xu JU, et al. Broadening the valid temperature range of optical thermometry through dual-mode design. J Mater Chem C. 2018;6(41):11178–83.
10. Gao Y, Huang F, Lin H, Zhou JC, Xu J, Wang YS. A novel optical thermometry strategy based on diverse thermal response from two intervalence charge transfer states. Adv Funct Mater. 2016;26(18):3139–45.
11. Brites CDS, Xie XJ, Debasu ML, Qin X, Chen RF, Huang W, et al. Instantaneous ballistic velocity of suspended Brownian nanocrystals measured by upconversion nanothermometry. Nat Nanotechnol. 2016;11(10):851–6.
12. Cai PQ, Wang XF, Seo HJ. Excitation power dependent optical temperature behaviors in Mn^{4+} doped oxyfluoride $Na_2WO_2F_4$. Phys Chem Chem Phys. 2018;20(3):2028–35.
13. Puddu M, Mikutis G, Stark WJ, Grass RN. Submicrometer-sized thermometer particles exploiting selective nucleic acid stability. Small. 2016;12(4):452–6.
14. Wang XF, Wang Y, Yu JH, Bu YY, Yan XH. Modifying phase, shape and optical thermometry of $NaGdF_4$:2%Er^{3+} phosphors through Ca^{2+} doping. Opt Express. 2018;26(17):21950–9.
15. Wang JM, Lin H, Cheng Y, Cui XS, Gao Y, Ji ZL, et al. A novel high-sensitive upconversion thermometry strategy: utilizing synergistic effect of dual-wavelength lasers excitation to manipulate electron thermal distribution. Sensor Actuat B Chem. 2019;278:165–71.
16. Suo H, Zhao XQ, Zhang ZY, Wu YF, Guo CF. Upconverting $LuVO_4$:Nd^{3+}/Yb^{3+}/Er^{3+}@SiO_2@Cu_2S Hollow Nanoplatforms for Self-monitored photothermal ablation. ACS Appl Mater Interfaces. 2018;10(46):39912–20.
17. Wu YF, Suo H, He D, Guo CF. Highly sensitive up-conversion optical thermometry based on Yb^{3+}-Er^{3+} codoped $NaLa(MoO_4)_2$ green phosphors. Mater Res Bull. 2018;106:14–8.
18. Yuan N, Liu DY, Yu XC, Sun HX, Ming CG, Wong WH, et al. A biological nano-thermometer based on ratiometric luminescent Er^{3+}/Yb^{3+}-codoped $NaGd(WO_4)_2$ nanocrystals. Mater Lett. 2018;218:337–40.
19. Meng QY, Liu T, Dai JQ, Sun WJ. Study on optical temperature sensing properties of YVO_4:Er^{3+}, Yb^{3+} nanocrystals. J Lumin. 2016;179:633–8.
20. Lei RS, Liu X, Huang FF, Deng DG, Zhao SL, Xu H, et al. Optical thermometry based on anomalous temperature-dependent 1.53 μm infrared luminescence of Er^{3+} in $BaMoO_4$: Er^{3+}/Yb^{3+} phosphor. Opt Mater. 2018;86:278–85.
21. Feng ZH, Lin L, Wang ZZ, Zheng ZQ. Low temperature sensing behavior of upconversion luminescence in Er^{3+}/Yb^{3+} co-doped PLZT transparent ceramic. Opt Commun. 2017;399:40–4.
22. Senapati S, Nanda KK. Red emitting Eu:ZnO nanorods for highly sensitive fluorescenceintensity ratio based optical thermometry. J Mater Chem C. 2017;5(5):1074–82.
23. Xu W, Cui Y, Hu YW, Zheng LJ, Zhang ZG, Cao WW. Optical temperature sensing in Er^{3+}-Yb^{3+} codoped $CaWO_4$ and the laser induced heating effect on the luminescence intensity saturation. J Alloy Comp. 2017;726:547–55.
24. Du P, Luo LH, Su J. Controlled synthesis and upconversion luminescence of Tm^{3+}-doped $NaYbF_4$ nanoparticles for non-invasion optical thermometry. J Alloy Comp. 2018;739:926–33.
25. Mukhopadhyay L, Rai VK, Bokolia R, Sreenivas K. 980 nm excited Er^{3+}/Yb^{3+}/Li^{+}/Ba^{2+}: $NaZnPO_4$ upconverting phosphors in optical thermometry. J Lumin. 2017;187:368–77.
26. Ma Y, Xiang G, Zhang J, Liu Z, Zhou P, Liu W, et al. Upconversion properties and temperature sensing behaviors in visible and near-infrared region based on fluorescence intensity ratio in $LuVO_4$: Yb^{3+}/Er^{3+}. J Alloys Compd. 2018;769:325–31.
27. Huo LL, Zhou JJ, Wu RZ, Ren JF, Zhang SJ, Zhang JJ, et al. Dual-functional β-$NaYF_4$: Yb^{3+}, Er^{3+} nanoparticles for bioimaging and temperature sensing. Opt Mater Express. 2016;6(4):1056–64.
28. Qin W-P, Liu Z-Y, Sin C-N, Wu C-F, Qin G-S, Chen Z, et al. Multi-ion cooperative processes in Yb^{3+} clusters. Light: Sci Appl. 2014;3(8):e193.
29. Zhang JH, Hao ZD, Li J, Zhang X, Luo YS, Pan GH. Observation of efficient population of the red-emitting state from the green state by non-multiphonon relaxation in the Er^{3+}–Yb^{3+} system. Light: Sci Appl. 2015;4(1):e239.
30. Suo H, Guo CF, Li T. Broad-scope thermometry based on dual-color modulation up-conversion phosphor $Ba_5Gd_8Zn_4O_{21}$:Er^{3+}/Yb^{3+}. J Phys Chem C. 2016;120(5):2914–24.
31. Wu H, Hao ZD, Zhang LL, Zhang X, Xiao Y, Pan GH, et al. Er^{3+}/Yb^{3+} codoped phosphor $Ba_3Y_4O_9$ with intense red upconversion emission and optical temperature sensing behavior. J Mater Chem C. 2018;6(13):3459–67.
32. Wang XF, Wang YM, Bu YY, Yan XH, Wang J, Cai PQ, et al. Influence of doping and excitation powers on optical thermometry in Yb^{3+}-Er^{3+} doped $CaWO_4$. Sci Rep. 2017;7:43383.
33. Wang R, Zhang X, Zhang Z, Zhong H, Chen Y, Zhao E, et al. Modified FIR thermometry for surface temperature sensing by using high power laser. Opt Express. 2017;25(2):848–56.
34. Jiang S, Zeng P, Liao L, Tian S, Guo H, Chen Y, et al. Optical thermometry based on upconverted luminescence in transparent glass ceramics containing $NaYF_4$:Yb^{3+}/Er^{3+} nanocrystals. J Alloys Compd. 2014;617:538–41.
35. Rakov N, Maciel GS. Exploring the $^4I_{13/2}$→$^4I_{15/2}$ radiative transition from Er^{3+} in Y_2O_3 for temperature sensing. J Lumin. 2018;199:293–7.
36. Wang XF, Liu Q, Bu YY, Liu CS, Liu T, Yan XH. Optical temperature sensing of rare-earth ions doped phosphors. RSC Adv. 2015;5(105):86219–36.

How to cite this article: Xiang G, Liu X, Liu W, et al. Multifunctional optical thermometry based on the stark sublevels of Er^{3+} in CaO-Y_2O_3: Yb^{3+}/Er^{3+}. *J Am Ceram Soc*. 2020;103:2540–2547. https://doi.org/10.1111/jace.16939